Parametric Dependencies of Sliding Window Correlation

Sadia Shakil ⬛, Jacob C. Billings, Shella D. Keilholz, *Member, IEEE*, and Chin-Hui Lee, *Fellow, IEEE*

Abstract— *Objective:* **In this paper, we explore the dependence of sliding window correlation (SWC) results on different parameters of correlating signals. The SWC is extensively used to explore the dynamics of functional connectivity (FC) networks using resting-state functional MRI (rsfMRI) scans. These scanned signals often contain multiple amplitudes, frequencies, and phases. However, the exact values of these parameters are unknown. Two recent studies explored the relationship of window length and frequencies (minimum/maximum) in the correlating signals.** *Methods:* **We extend the findings of these studies by using two deterministic signals with multiple amplitudes, frequencies, and phases. Afterward, we modulate one of the signals to introduce dynamics (nonstationarity) in their relationship. We also explore the relationship of window length and frequency band for real rsfMRI data.** *Results:* **For deterministic signals, the spurious fluctuations due to the method itself minimize, and the SWC estimates the stationary correlation when frequencies in the signals have specific relationship. For dynamic relationship also, the undesirable frequencies were removed under specific conditions for the frequencies. For real rsfMRI data, the SWC results varied with frequencies and window length.** *Conclusion:* **In the absence of any "ground truth" for different parameters in real rsfMRI signals, the SWC with a constant window size may not be a reliable method to study the dynamics of the FC.** *Significance:* **This study reveals the parametric dependencies of the SWC and its limitation as a method to analyze dynamics of FC networks in the absence of any ground truth.**

Index Terms—**Dynamics, frequency, sliding window correlation, sliding window covariance, stationary.**

I. INTRODUCTION

RESTING-STATE functional MRI (rsfMRI) is a successful tool for the study of normal and disordered brain function

[1], [2]. The functional connectivity (FC) networks formed by coordinated activation of various regions in the resting brain are non-stationary and change state or configuration within seconds. These dynamics may contain the key to understand intrinsic brain functions and many recent studies focus on their comprehension [3]–[6]. Despite the importance of these dynamics, the choice of the suitable analysis method for their study is a big challenge due to lack of any ground truth (GT) [7]. Sliding window correlation (SWC) is the simplest and most commonly used method for dynamic FC analysis and most of the dynamic FC studies use it at some point [3]–[5], [8]–[16]. In the SWC, a temporal window of a certain size and shape is selected, and the correlation coefficient between two signals of interest within that window is computed. The process is repeated for the entire scan length by shifting (sliding) the window by certain offset [7].

Results of the SWC are strongly influenced by the window length [3], [7], [12], [14], [17] which can be influenced by the amplitudes, frequencies, and phases of the correlating signals. Deciding the best window length in the absence of any GT is highly desirable but not easy. Studies have suggested alternate methods of exploring these dynamics [9], [18], [19] and some have proposed new methods, too [20], [21]. One recent study [22] also suggested to use stationary as well as SWC analysis jointly for more reliable results. However, the SWC remains one of the most widely used method in latest fMRI [23]–[30] and non-fMRI studies [31]–[33].

The vast use of the SWC emphasizes on the need to explore the performance of the SWC from different angles. Some recent studies focused on detailed analysis of the SWC [7], [34] and some others explored the best window size for the SWC, too [9], [12], [15], [17]. However, the detailed mathematical break down of the SWC and subsequent guidance for the dependence of minimum window length on the minimum frequency of correlating signals is explained extensively in [6] only. In an extension of this study, [5] explored the influence of both the minimum and the maximum frequency components in the correlating signals. Studies have started to follow these guidelines [26]–[29], however, there is still a need for comprehensive analysis of the SWC dependence on multiple amplitudes, frequencies, and phases of the correlating signals. Furthermore, the dependence of the SWC on these parameters in real resting-state data needs to be explored, too. A preliminary version of the current study is published in [5] and here we are extending it to the signals with multiple frequency components separated by multiple phase lags and having different amplitudes along

with real resting-state data. We start the analysis with the study of sliding window covariance, and extend it to the SWC. Similar to [6] and [5] the influence of dynamic (non-stationarity) relationship between the two signals is also explored.

The rest of the paper is arranged as follows: Section II provides an in-depth discussion of sliding window covariance (SWCov) for deterministic signals and explains the relationship between sliding window covariance and correlation. Section III explores the SWCov for dynamic (non-stationary) relationship of the signals in the frequency domain. Section IV reports SWC results for real resting-state networks. Finally we discuss our findings and present some future work in Section V followed by the conclusion in Section VI. Supplementary file (provided separately) contains detailed derivations of our study.

II. DETERMINISTIC SIGNALS

The sliding window correlation coefficient of two signals x and y at time point n is given by:

$$\rho_{xy}[n] = \frac{c_{xy}[n]}{\sqrt{c_{xx}[n]}\sqrt{c_{yy}[n]}} \tag{1}$$

which is SWCov $c_{xy}[n]$, normalized by the standard deviations $\sqrt{c_{xx}[n]}$ and $\sqrt{c_{yy}[n]}$ [6]. The SWCov between the two signals within the window w is given by:

$$c_{xy}[n] = \left(\frac{TR}{w}\right) \sum_{i=n-\Delta}^{i=n+\Delta} x_i y_i - \overline{y}_n \overline{x}_n \tag{2}$$

in which $w = (2\Delta + 1)TR$ is the odd window length in seconds, TR is the sampling or repetition time of the scans, and $\overline{x}_n$, $\overline{y}_n$ are means of the signals x and y respectively for the window positioned at n [6]. We start with SWCOv and then work on the SWC as explained in Section II-C.

A. Multiple Amplitudes, Frequencies, and Phases

We use two deterministic signals composed of sinusoids that are sum of multiple amplitudes, frequencies, and phases. We select these signals as an extension of [5] and also since real-world signals can be approximated by sum of sinusoids [35]. The first signal x_i consists of sum of m sinusoids with m distinct frequencies and amplitudes. The second signal y_i consists of sum of sinusoids with same amplitudes and frequencies but differing in phases from sinusoids of x_i. Since the correlating signals are bandpass filtered (normally 0.01–0.08 Hz or 0.01–0.1 Hz) for real resting-state scans we also assume that these m frequencies lie between f_{min} (0.01 Hz) and f_{max} (0.08 or 0.1 Hz) such that $f_{min} = f_1 < f_2 < ... < f_m = f_{max}$. Furthermore, the real resting-state signals have power spectral density $S(f) = \frac{1}{f^2}$, at frequency f. In order to have signals with frequency spectra close to real resting-state signals we choose the amplitudes of the sinusoids decaying as $\frac{1}{f^2}$ such that $A_{max} = (\frac{1}{f_{min}^2}) = A_1 > A_2 > ... > A_m = A_{min} = (\frac{1}{f_{max}^2})$. The correlating
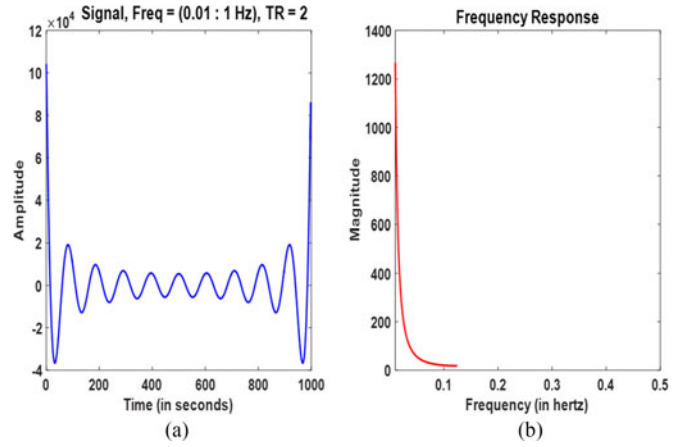

Fig. 1. (a) Sum of sinusoids with increasing frequencies and decaying amplitudes. (b) Frequency spectrum of the signal.

signals x_i and y_i can be written as:

$$x_i = \sum_{j=1}^{m} A_j \cos(2\pi f_j i TR)$$

$$y_i = \sum_{j=1}^{m} A_j \cos(2\pi f_j i TR + \theta_j) \tag{3}$$

Fig. 1. shows the plot of x_i composed of sinusoids with different frequencies and amplitudes along with corresponding frequency spectrum. It can be observed that the amplitude of the signal decays as $\frac{1}{f^2}$.

Using (2), the SWCov of these two signals for the window positioned at n would be given by:

$$c_{xy}[n] = \sum_{j=1}^{m} \frac{A_j^2}{2} \cos(\theta_j) + \left(\frac{1}{4\pi w}\right)(E) + \left(\frac{2}{\pi w}\right)(F)$$

$$+ \left(\frac{2}{\pi w}\right)(G) - \left(\frac{1}{\pi^2 w^2}\right)(H) \tag{4}$$

The detail derivation of the above equation for the values of E, F, G, and H are available in the Supplementary file. Since the two signals are deterministic so their relationship is not dynamic. Consequently, the SWCov (SWC) is expected to be the same as stationary covariance (correlation) in every window regardless of the window size. However, it can be observed from (4) that the results are dependent on the size of the window (w) as discussed below.

1) Infinite Window Length: Stationary covariance over the entire signal length would be obtained from (4) when $w \rightarrow +\infty$ [6], and the value of the stationary covariance would be:

$$\lim_{w \rightarrow +\infty} c_{xy}[n] = \sum_{j=1}^{m} \frac{A_j^2}{2} \cos(\theta_j) \tag{5}$$

2) Finite Window Length: For window length (w) spurious fluctuations would be introduced from last four terms in (4). As a result, the covariance over the finite window w would approach the stationary covariance when these terms are zero
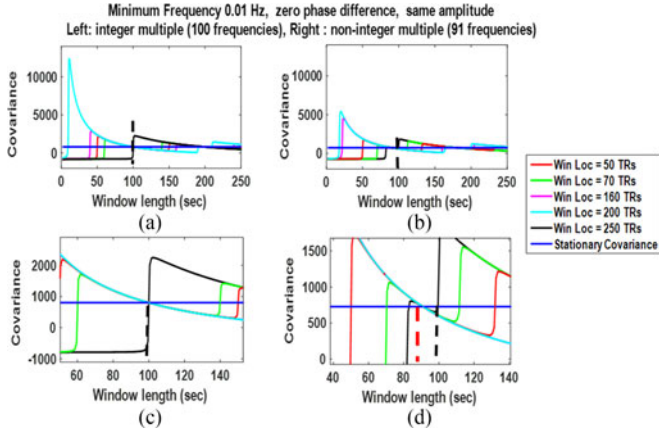
Fig. 2. Sliding window covariance of deterministic signals with multiple frequency components for different window locations (Win Loc). (a) When all the higher frequencies are integer multiples of the minimum frequency and (b) when they are not integer multiples. (c) is zoomed in view of (a) and (d) which is zoomed in view of (b). In (d) the sliding window covariances are converging to stationary covariance for a window (vertical red line) other than the minimum window length (vertical black line).

(*i.e.*, E, F, G, and $H = 0$) resulting in (Supplementary file for details):

$f_j = l_j f_1$, in which $j = 2, 3....m$ and $l_j > 1$.

It shows that all the frequencies can be expressed as multiples of the minimum frequency f_1. Putting all the higher frequencies as multiples of lowest frequency f_1 can have two possibilities (Supplementary file for details).

1) *Case 1:* f_j is an integer multiple of f_1, $j = 2,3...m$

   In this case only the first term $\sum_{j=1}^{m} \frac{A_j^2}{2} \cos(\theta_j)$ in (4) will be non-zero and the SWCov would approach the stationary covariance similar to the results of [6] and [5].

2) *Case 2:* f_j is an not an integer multiple of f_1, $j = 2,3...m$
   This would result in last four terms of (4) to be zero only when w cancels out all multiples of f_1 in arguments of all $sin()$ functions (Supplementary file for details). In the absence of such a window length the SWCov would not be able to estimate the stationary covariance reliably.

From these observations we conclude that for deterministic signals comprising the sum of sinusoids the SWCov would be able to estimate the stationary (real) covariance for a window of length $\frac{1}{f_{min}}$ (or at its integer multiples) only when all the higher frequencies are integer multiples of f_{min}. Otherwise, the window length w has to cancel out the non-integer multiples of f_{min} for all $sin()$ functions in (4).

The terms E, F, G, and H in (4) involve phase differences (θ s) indicating that the spurious fluctuations introduced by the SWCov would be dependent on the phase differences, too.

B. Results

Results for the dependence of SWCov on frequencies, phases, and amplitudes of the correlating signals are given below.

1) Frequency Dependence: Fig. 2. shows the plots when the deterministic correlating signals contain more than ninety frequency components that are integer multiples of the minimum
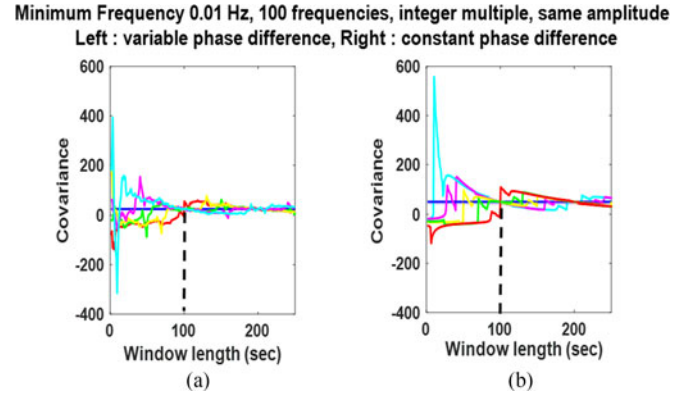

Fig. 3. Sliding window covariance of deterministic signals with multiple frequencies and non-zero phase difference for different window locations. Phase difference is varibale in (a) and is constant in (b).
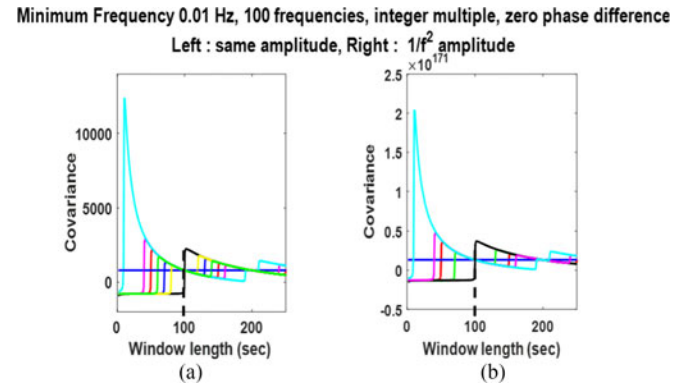

Fig. 4. Sliding window covariance of deterministic signals with different amplitudes. In (a) amplitudes are same and in (b) the amplitudes are changing as $\frac{1}{f^2}$.

frequency in (a) and not integer multiples in (b). Plots (c) and (d) are zoomed in version of the plots above them.

We plot the results for various window locations to evaluate if the SWCov reliably estimates stationary covariance for all window locations when $w \geq \frac{1}{f^2}$ as reported in [6]. In both of these cases the minimum frequency is at 0.01 Hz, phase differences are zero, and sinusoids have same amplitudes. It can be observed ((a) and (c)) that the SWCov reliably estimates the stationary covariance (black horizontal line) when the minimum window length is $\frac{1}{f_{min}}$ (vertical black line) for all window locations. However, this is not the case when the frequencies are not integer multiple of f_{min} as shown in (b) and (d).

2) Phase Dependence: Fig. 3. shows influence of non-zero phase difference on the results of the SWCov. The f_{min} is 0.01 Hz, all frequencies are integer multiple of f_{min}, and all sinusoids have same amplitudes. Fig. 3. contains plots for variable phase differences in (a) and constant one in (b). The SWCov results estimate the stationary covariance reliably in both cases, however, constant phase difference resulted in smoother SWCov time course as seen in (b).

3) Amplitude Dependence: Fig. 4. shows influence of changing the amplitudes of the sinusoids. In (a) amplitudes are same and in (b) the amplitudes are changing as $\frac{1}{f^2}$. In both of these cases the minimum frequency is at 0.01 Hz, all phases are
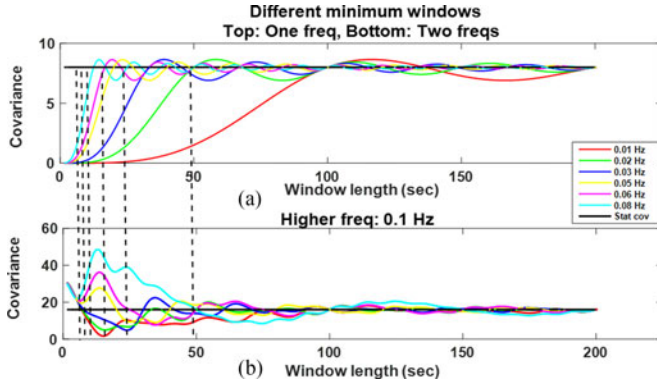
Fig. 5. Sliding window covariance of deterministic signals with zero phase difference, and different minimum frequencies. The correlating signals have just f_{min} in (a) and have two frequencies in (b).

taken to be zero, and higher frequencies are integer multiples of f_{min}. It can be observed that the values of SWCov is different in both cases, however, the pattern of values is the same and it is estimating stationary covariance (black horizontal line) when $w = \frac{1}{f_{min}}$.

4) Minimum-Frequency Dependence: Fig. 5. shows the influence of different minimum frequencies in the correlating signals. The phase difference is zero here, amplitudes are constant, and the window is placed at the same location for all of these plots. However, the minimum bandpass cutoffs are different for each case (0.01, 0.02, 0.05, 0.06, and 0.08 Hz). These frequencies correspond to minimum window length (to estimate the stationary correlation) ranging from 12.5 to 100 seconds. Plots in (a) correspond to the minimum window length for each of above mentioned frequencies when both the correlating signals contain just the f_{min} sinusoid. In (b) the window lengths are same as in (a) but a frequency other than the minimum frequency (not necessarily an integer multiple of the minimum frequency) is added. It can be observed that in (a) the SWCov is estimating the stationary covariance (horizontal black line) accurately at the minimum window lengths (black vertical lines). However, it fails to do so in (b) if the higher frequency was not an integer multiple of the lower frequency. Hence, addition of just one frequency is influencing the estimation properties of the SWCov.

C. Sliding Window Correlation

The SWC is the SWCov normalized by the standard deviations $\sqrt{c_{xx}[n]}$ and $\sqrt{c_{yy}[n]}$ as shown in (1) over each window. To avoid further complexity we are not giving the details of these terms here. However, similar to the terms in SWCov, standard deviations would involve one term independent of window length and the rest would be dependent on the window length. They would normalize the stationary covariance for an infinite window and would influence the spurious fluctuations for finite windows similar to [6]. So, overall the SWC would follow the same pattern as sliding window covariance but the values would be normalized between -1 and 1. Hence, for finite windows, similar to the SWCov, the SWC would reliably estimate the

stationary correlation (for windows which are an integer multiple of $\frac{1}{f_{min}}$) only if all the higher frequencies are an integer multiple of the f_{min} for sum of sinusoids.

III. MODULATED SIGNAL (DYNAMIC RELATIONSHIP)

The SWC is expected to capture the dynamics of the FC in the real rsfMRI signals. Until this point in our study we focus on exploring the inherent limitations of the SWC process itself by using deterministic signals. However, in next part of the study we investigate the efficiency of the SWC to capture the dynamics of the relationship between correlating signals. Similar to [6] and [5] we modulate one of our signals with low frequency sinusoids in order to introduce dynamics (non-stationarity) in their relationship. For this purpose, we multiply the signal y_i with two modulating signals $\cos(2\pi f_{01} i TR)$ and $\cos(2\pi f_{02}) i TR$, in which $f_2 > f_1 >> f_{02} >> f_{01}$. In order to reduce the complex computations we are taking only two frequencies ($f_1 = f_{min}$ and $f_2 = f_{max}$) for both x_i and y_i. We also assume the zero phase difference between the two signals. The modulated signal y_i is given by:

$$y_i = \{(A_1 \cos(2\pi f_1 i TR) + A_2 \cos(2\pi f_2 i TR))\}$$
$$\cos(2\pi f_{01} i TR) \cos(2\pi f_{02} i TR) \quad (6)$$

From the above equation it is evident that the desired non-stationarity (dynamics) in the relationship between the two signals is introduced by two frequencies: $f_{03} = f_{02} + f_{01}$ and $f_{04} = f_{02} - f_{01}$ and SWCov (SWC) should be able to extract these frequencies only. Solving for covariance in Fourier domain (Supplementary file for details) we conclude that in the presence of dynamics (introduced by modulation of one signal) the higher frequency f_2 needs to be above a certain multiple of the lower frequency f_1 ($f_2 - f_{03} > 2f_1$). Otherwise, frequencies other than the desirable dynamics (comprising the frequency components f_{03} and f_{04}) would be captured by SWCov (SWC).

A. Results

It can be observed from Fig. 6. that frequency components other than the desirable frequencies are retrieved when above mentioned condition in Section III is not met. These frequencies are introduced due to aliasing of frequencies when $f_2 - f_{03} < 2f_1$.

IV. SLIDING WINDOW CORRELATION FOR REAL DATA

Until this point this study was focused on exploring influence of various parameters on the SWC results for correlating sinusoids. However, real rsfMRI data is not expected to be composed of simple sinusoids (even though it can almost always be approximated by sum of sinusoids [35]). This section explores the dependence of the SWC results on different parameters of the correlating signals from real resting-state data.

A. Data and Preprocessing

We used rsfMRI scans of nine healthy human subjects (four females, ages: 21–57 years, downloaded from
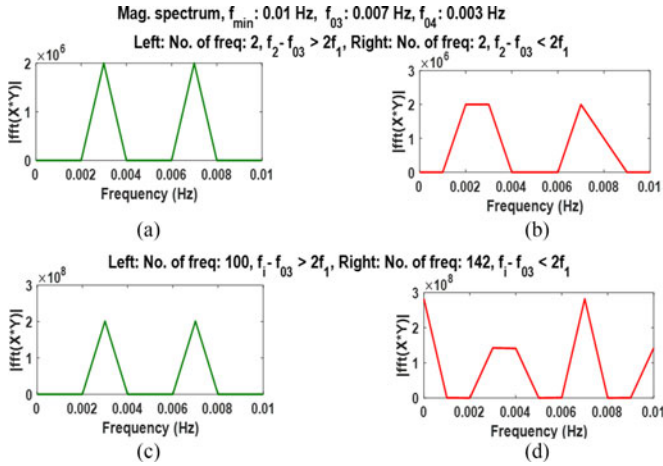
Fig. 6.   Plots of the SWC for signals with two frequency components when (a) $f_2 - f_{03} > 2f_1$ and (b) $f_2 - f_{03} < 2f_1$ and for 100 frequency components when (c) $f_i - f_{03} > 2f_1$ and (d) $f_i - f_{03} < 2f_1$. Undesirable frequency components can be noticed in (b) and (d).
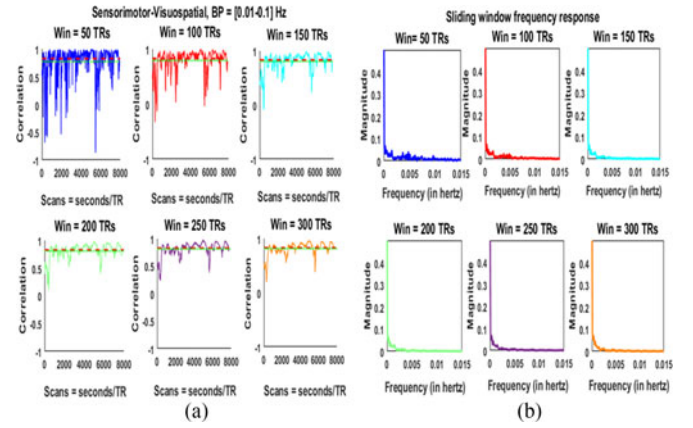

Fig. 7.   (a) Stationary correlation (red), mean sliding window correlation (green), and sliding window correlations for different windows. (b) Frequency spectrum of the results in (a).

(http://www.nitrc.org/projects/fcon_1000/). The scans were done on SIEMENS MAGNETOM TrioTim syngo MR B17 scanner. The scanning parameters were: TR = 645 ms, voxel size = 3mm isotropic, duration = 10 min, TE = 30 ms, slices = 40, multi-band accel. factor = 4, time points = 900. Initial 10 volumes of each scan were discarded to compensate for transient scanner instability. All preprocessing was done in statistical parametric mapping toolbox (SPM 12, http://www.fil.ion.ucl.ac.uk/spm/). Preprocessing included motion correction, coregisteration of the functional images with the anatomical image, segmentation, normalization, and smoothing. Default parameter values from SPM12 were used during preprocessing but smoothing was done using a Gaussian kernel of size 8 and for normalization a voxel size of 3x3x3 was chosen. The images were co-registered to the AAL atlas [36] using nearest neighbor interpolation without any warping. After preprocessing, four functional networks (Dorsal DMN, Ventral DMN, Visuospatial, and Sensorimotor) were extracted from gray matter regions using the masks from the Stanford's functional imaging in neuropsychiatric disorders (FIND, http://findlab.stanford.edu/home.html) lab [37] for all subjects.

B. Network Time Series

In order to perform the SWC, we formed the time series of the four networks mentioned above (Section IV-A) by using the masks given in [37] for all nine subjects. Time series of each network was formed by taking the mean of all of its voxels' intensities at every time point. Time series of each network for all the subjects were zscored and then concatenated. All the analysis reported in this study was done on the zscored concatenated time series for two of the four networks (Sensorimotor and Visuospatial) after band pass filtering them (0.01–0.1 Hz, FIR, order 80). However, similar results were obtained for the analysis with any two of the four networks. The filtered band of frequencies was 0.01–0.1 Hz unless otherwise specified.

C. Sliding Window Correlation and Frequency Response

We estimated the SWC and corresponding magnitude spectrum for six windows (50, 100, 150, 200, 250, and 300 TRs). In this case the minimum window length to avoid spurious fluctuations [5], [6] would be 100 seconds (155 TRs). We selected window sizes below (50 and 100 TRs), above (200, 250, and 300 TRs) and almost equal (150 TRs) to this size. Fig. 7. shows the results of the SWC in (a) and corresponding frequency responses in (b).

Each plot in (a) also has stationary correlation value (in red) and mean of the SWC (in green). As expected the SWC time courses have higher frequencies for smaller windows (below 150 TRs) and lower for larger windows. Frequency spectrum plots in (b) have significant amount of power (magnitude) at the frequencies below f_{min} (0.01 Hz) which may be the result of dynamics (non-stationarity) in the FC as reported in [6]. However, the frequencies containing significant powers are dependent on the window length also since a sliding window acts as a low pass filter with cutoff at $\frac{1}{w}$.

D. Dependence on Window Position

In [6] it was reported that the SWC would estimate the stationary correlation (for sinusoids) or mean of the SWC (for real resting-state data) for any window position provided that the size of window is larger than $\frac{1}{f_{min}}$.

We explored this result for our data by changing the position of the window and the results are shown in Fig. 8. We placed the windows (a) at the start, (b) in the middle, and (c) at the end of the concatenated time series. The spurious fluctuations diminish with the increase in window size and SWC results converge very close to a value (mostly the mean of the SWC plotted in blue). However, the convergence is not at $w = \frac{1}{f_{min}}$ (black vertical lines) but at some other window size (green dashed vertical lines) always larger than $\frac{1}{f_{min}}$. The exact size of this window is not evident but it falls within a range (between 200 and 250 TRs in Fig. 8).

The SWC results do not converge to stationary correlation (red horizontal lines) which shows that stationary correlation
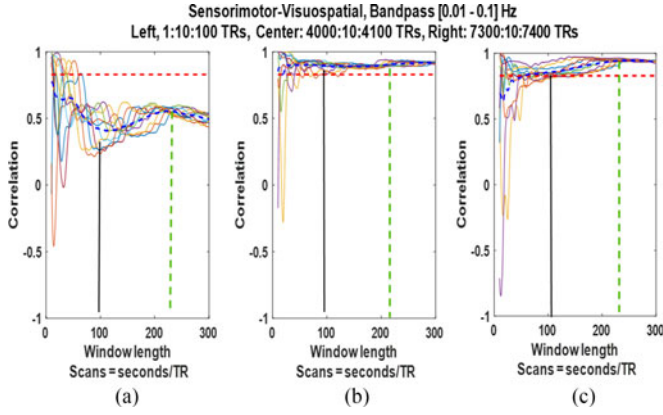
Fig. 8. Sliding window correlation of the bandpass filtered (0.01–0.01 Hz) signals for three different sets of window positions.
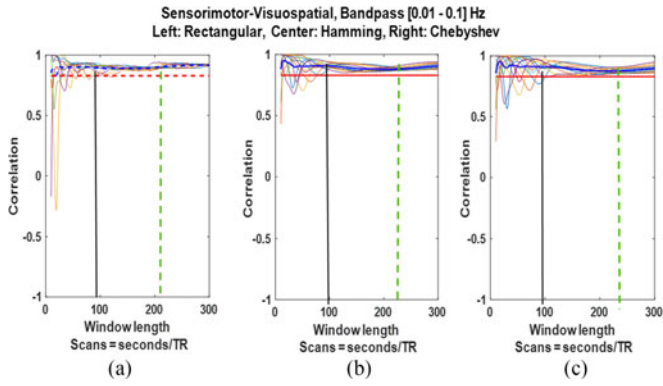

Fig. 9. Sliding window correlation results for different window positions using (a) rectangular, (b) Hamming, and (c) Chebyshev windows.

is not the true representative of the relationship between two time series for short time scale [22]. These results show that the spurious fluctuations arising from the SWC reduce significantly for larger windows ($w \geq \frac{1}{f_{min}}$) and exact size of this window is difficult to find. However, range of this window size can be estimated which may be used for dynamic FC analysis in the absence of some better method of estimating the best and maybe adaptive window size.

E. Dependence on Window Type

We also estimated the SWC using tapered windows (Hamming and Chebyshev) and the results are shown in Fig. 9. It can be seen that the tapered windows provide smoother results as expected, however, the change in window type does not change the convergence point of the SWC to $\frac{1}{f_{min}}$.

F. Dependence on Filter Type

In order to compute the influence of filter type on the SWC results, we compared the results of bandpass (0.01–0.1 Hz) and highpass (0.01 Hz) filtered time series of the two networks. Fig. 10. shows the results of application of these two filters. It can be observed that in both cases the SWC converges to the same correlation values for windows larger than 100 seconds
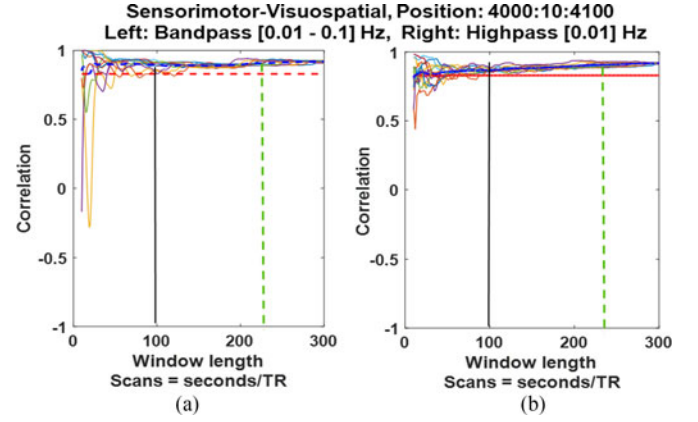

Fig. 10. Sliding window correlation of the (a) bandpass filtered (0.01–0.1 Hz) and (b) highpass filtered (0.01 Hz) time series.
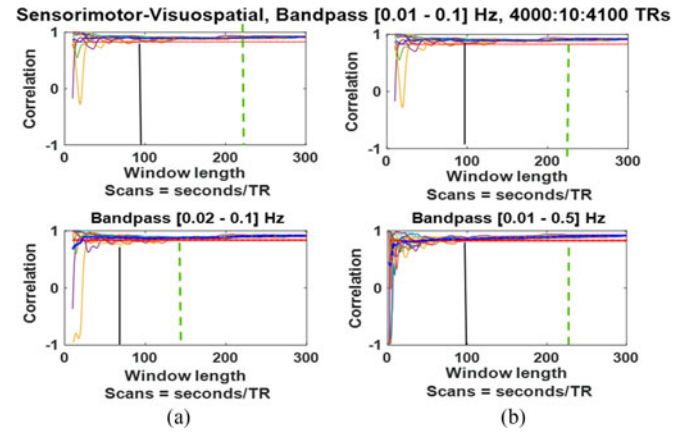

Fig. 11. Changing the lower (a, bottom row) or upper (b, bottom row) cutoff of the frequency band influences the convergence of the sliding window correlation results.

(155 TRs), however, inclusion of higher frequencies reduced the spurious fluctuations.

G. Dependence on Bandpass Cutoffs

We observed the influence of change in the bandpass cutoff by changing only the lower cutoff in Fig. 11. (a, bottom row) and only the higher cutoff in Fig. 11. (b, bottom row) from the cutoffs we used before (0.01–0.1 Hz, top row). We are taking the window positions that provided the best (fastest) convergence (in Section IV-F) to compare these results. Reducing the lower cutoff in ((a), bottom) moves minimum window length to avoid spurious fluctuations from 100 seconds (155 TRs) to 62.5 seconds (97 TRs). It can be observed that in this case the SWC convergence point changes with the change in frequency band. It shows that the frequency band of the correlating signals (and not the minimum frequency only) plays an important part in deciding the best window length.

H. Dependence on Network

We picked two different sets of networks (Sensorimotor, Visuospatial and Dorsal DMN, Ventral DMN) in order to see if the
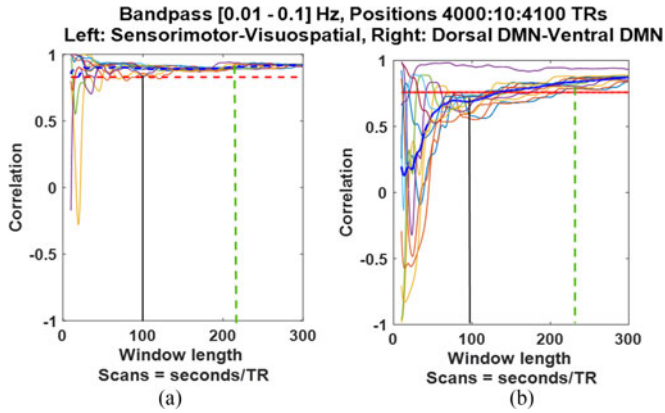
Fig. 12.   Sliding window correlation results changed based on the correlating networks.
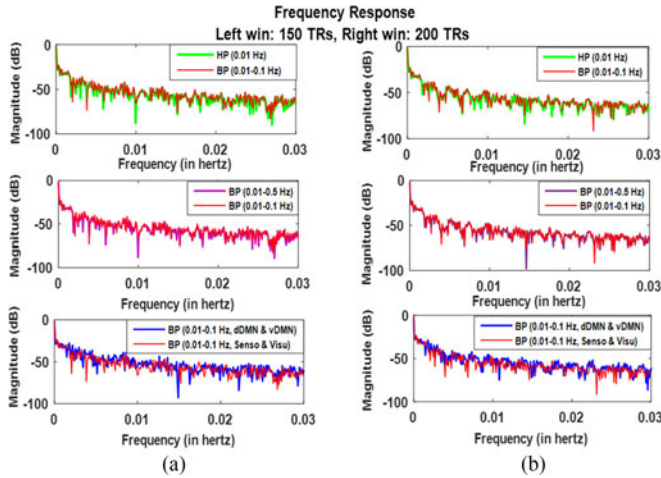

Fig. 13.   Comparison of frequency response of the SWC results under different conditions for (a) 150 TRs window and (b) 200 TRs window. Minimum cutoff for all cases is 0.01 Hz.

selection of network influences the SWC results. It can be seen from Fig. 12. that change in the network pair does influence the convergence of the SWC.

I. Frequency Response Comparison

In [6] it was reported that dynamics (non-stationarities) of the FC are captured in the SWC results below f_{min} if ($w \geq \frac{1}{f_{min}}$). [5] reported that there has to be a specific relationship between higher and lower frequencies to achieve this result. We explored this result for real resting-state data under different conditions. Fig. 13. shows the results for (a) 150 TRs and (b) 200 TRs windows. First row is the frequency response (in dB) for bandpass (red) and highpass (green) filtered signals. It can be observed that in both the cases major power (magnitude) lies below 0.01 Hz (lower cutoff) which may be due to dynamics (non-stationary) in the FC. However, the power is greater for highpass which may be the result of some undesirable frequency components. Similar results were obtained for comparison of different frequency bands in second row and different network pairs in third row.
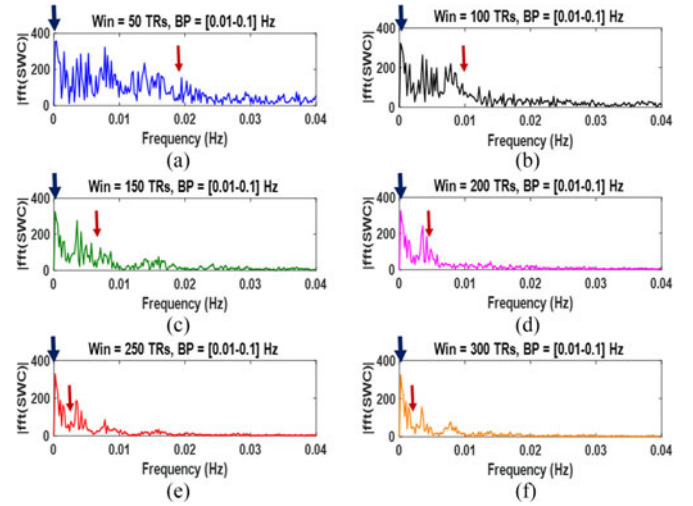

Fig. 14.   Magnitude spectrum for different windows having different low pass cutoffs (red arrows). The non-stationarities (dynamics) stabilize for best window range in (e) and (f).

J. Capturing Dynamics

In [6] it was reported that the SWC results would capture the non-stationarities of the correlating signals which are below f_{min} for a window of size $\geq \frac{1}{f_{min}}$. However, our results show that increasing the size of the window would decrease the extracted non-stationarities since SWC acts as low pass filter with the cutoff equal to $\frac{1}{w}$. Fig. 14. shows these cutoff frequencies (red arrows) for different window lengths.

This figure also shows the magnitude spectrum (blue arrows, after subtraction of mean SWC) that contributes the most and does not decay much with the increase in window length. Furthermore, the pattern of non-stationarities remains the same for the estimated best window range (between 200 and 250 TRs). This may be since the undesirable non-stationarities are rejected for these windows and the non-stationarities captured maybe due to the actual dynamics of the correlating signals.

K. Means of all Network Pairs

To summarize our results we computed the means of results for all six network pairs of the four networks (Sensorimotor, Visuospatial, dorsal DMN, and ventral DMN). In order to observe how much the SWC differs from the stationary and mean SWC over the whole scan length, we computed the difference of the SWC for each window (50, 100, 150, 200, 250, and 300) and all frequency bands (0.01–0.1 Hz, 0.01–0.5 Hz, 0.02–0.1 Hz, and 0.1 Hz (highpass)) from stationary and mean SWC. We computed these differences for all network pairs and then computed means of absolute values of these differences. Fig. 15. shows the plots of these means for all windows and frequency bands. It can be observed that the mean is decreasing as the size of the window increases which is an expected result. It can also be observed that for each window the means for the difference from mean SWC and from stationary correlations are almost the same. This shows that even though the SWC estimates differ from the stationary correlations for the duration of the window, capturing
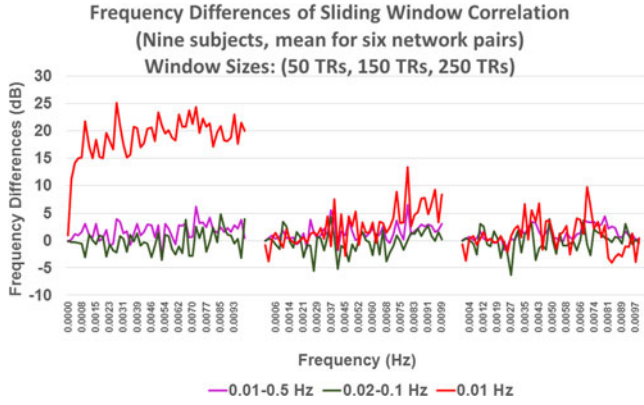
Fig. 15. Correlation difference of the sliding window correlation from mean sliding window correlation (left) and from stationary correlation (rigth).
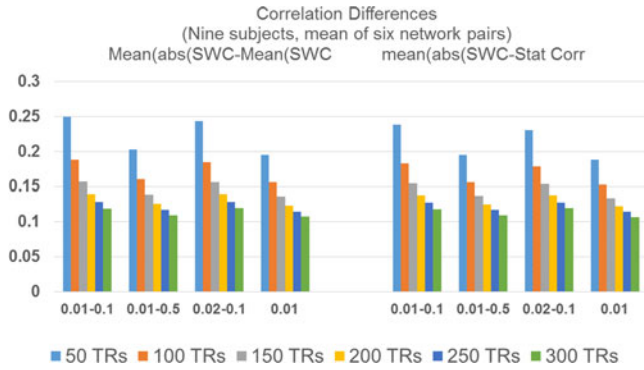

Fig. 16. Difference of frequency spectrum of SWC results of bandpass (0.01–0.1 Hz) filtered signals from signals with other frequency components.

the short lived relationship of the correlating signals, but the mean of SWC results over the entire scan length approaches the stationary correlation value.

Fig. 16. shows the difference (in dB) of the amplitude spectrum of different frequency bands (0.01–0.5 Hz, 0.02–0.1 Hz, and 0.01 Hz (highpass)) from the most commonly used frequency band (0.01–0.1 Hz) for rsfMRI data. The plots are means of all six network pairs and three windows (50 TRs, 150 TRs, 250 TRs) and the results are plotted from 0–0.01 Hz duration since this is the frequency band that should capture the non-stationarity of the correlating signals in the SWC results as mentioned in [6].

It can be seen that the amplitude differences for very low frequencies are small for larger windows (150 TRs, 250 TRs) for all frequency bands, however, they are not zeros for any case. These results indicate that changing the range of frequencies of the correlating signals would influence the frequency components of the resultant SWC time courses. In general higher power (amplitudes) are at the low frequencies (as shown in Fig. 13) but the power distribution changes with the change in frequencies. Furthermore, the difference is larger for highpass filtered data (red) for almost all the cases. From these results we can conclude that even though non-stationarity is captured in the SWC below the lower cutoff as reported in [6] but the exact frequency

distribution changes with frequency components. In the absence of any ground truth it can not be established if these variations are because of some undesirable frequency components or are capturing the true non-stationarity in the relationship of the two signals.

L. Phase Randomization

We generated surrogate time series of correlating signals by phase randomization [38]. The frequency responses and autocorrelation of the time series remained the same after randomization of the phases. The results showed a lot of spurious fluctuations even after the window size increased $\frac{1}{f_{min}}$. For frequency response also, we observed that the power at very low frequencies was almost 20-30 dB less than the power obtained for the same frequency band in original (non-randomized) data. As a result, we conclude that the results observed in our study are not by chance.

V. Discussion

In this study we analyzed the impact of various parameters on SWC results. We started with deterministic signals followed by modulating one of the signals to introduce dynamics in their relationship. Similar to the results of [6] and [5] the SWC approached the stationary correlation when w (window length) $\geq \frac{1}{f_{min}}$. However, the SWC estimated the exact stationary correlation value at this window (and at its integer multiples) only if the higher frequencies were integer multiples of the f_{min}. Furthermore, for dynamic relationship (in case of one modulated signal) we discovered that the SWC extracted undesirable frequency components if certain conditions were not met.

Similarly in real rsfMRI data also the SWC approached mean of the SWC when w (window length) $\geq \frac{1}{f_{min}}$. This converging window length was different for different positions of the window but it was between some window range (e.g., between 200 and 250 TRs for Sensorimotor and Visuospatial networks with $f_{min} = 0.01$ Hz). This may be because the relationship between any two networks may change at unequal intervals at different times and same window can not capture variable length dynamics. Defining a range of these windows may help in approximating the best window size for the analysis. Changing the filter from bandpass to highpass or even changing the bandpass cutoffs resulted in modification of the results, however, convergence always occurred for larger windows. Moreover, even for the same frequency band the SWC results were different for different network pairs. Study of the frequency response of the SWC results showed that most of the power (magnitude) lies below the lower cutoff of the filter for larger windows ($\geq \frac{1}{f_{min}}$) as reported in [6] and [5]. This power from some undesirable dynamics (introduced as a result of frequency components of the correlating signals) in addition to the desired dynamics. The power at very low frequencies remain stable for all windows.

In this study we are not focusing on the influence of many source of variations (such as noise, motion), but only on the influence of the SWC itself. These results clearly identify the fact that the results of the SWC are dependent on many factors and the current methods of choosing a window size may be

limiting the output of the method. Our study validates the results about the minimum window length to minimize the spurious fluctuations and frequency distribution of the SWC results in [6] and [5], however, it also shows that the SWC with one window length may not be able to capture the dynamics correctly. We may either define a range of window lengths or develop a better method of estimating the adaptive window length.

VI. CONCLUSION

For deterministic time series the SWC reliably estimated the stationary correlation when higher frequencies were integer multiple of the f_{min}. Furthermore, when the dynamics were introduced in the relationship of two signals, the SWC captured the modulating frequencies under specific conditions only. Similar results were observed for real rsfMRI data also and based on those results the following recommendations can be made for the choice of best window length:

1) The SWC should be estimated by placing the window at various locations and changing its size from very small to very large.
2) Range of window lengths providing the best estimate of the mean SWC should be noted.
3) The window in this range should be able to capture the true dynamics (non-stationarity) of the FC reliably and this can be confirmed by plotting the frequency spectrum of the result for different window lengths.
4) The non-stationarity captured can be used to study the dynamics of resting-state networks.

The SWC based studies may define a range of window sizes but this is still not the optimum way to capture FC dynamics. In future, studies may look into new ways of dynamic analysis of the FC. There are number of scenarios that can be explored for this purpose. One possibility can be to detect efficient window size by observing the peaks of cross correlation between the two correlating signals. The future work in this direction may also focus on the formation of some frequency dependent model by using some data driven method such as Hilbert-Huang Transform [39]. Another possibility can be to identify the change points of these networks adaptively by image processing of the rsfMRI scans [40]. Any two consecutive change points may represent the time of change in the network dynamics.

ACKNOWLEDGMENT

REFERENCES

[1] C. Sorg *et al.*, "Selective changes of resting-state networks in individuals at risk for alzheimer's disease," *Proc. Nat. Acad. Sci.*, vol. 104, no. 47, pp. 18 760–5, 2007.

[2] S. Rombouts *et al.*, "Altered resting state networks in mild cognitive impairment and mild alzheimer's disease: An fMRI study," *Hum. Brain Mapping*, vol. 26, no. 4, pp. 231–239, 2005.

[3] S. Keilholz *et al.*, "Dynamic properties of functional connectivity in the rodent," *Brain Connectivity*, vol. 3, no. 1, pp. 31–40, 2013.

[4] V. Kiviniemi *et al.*, "A sliding time-window ICA reveals spatial variability of the default mode network in time," *Brain Connectivity*, vol. 1, no. 4, pp. 339–347, 2011.

[5] S. Shakil *et al.*, "On frequency dependencies of sliding window correlation," in *Proc. Int. Conf. Bioinf. Biomed.*, 2015, pp. 363–368.

[6] N. Leonardi and D. Van De Ville, "On spurious and real fluctuations of dynamic functional connectivity during rest," *NeuroImage*, vol. 104, no. 1, pp. 430–436, 2015.

[7] S. Shakil *et al.*, "Evaluation of sliding window correlation performance for characterizing dynamic functional connectivity and brain states," *NeuroImage*, vol. 133, pp. 111–128, 2016.

[8] D. Schulz and J. Huston, "The sliding window correlation procedure for detecting hidden correlations: Existence of behavioral subgroups illustrated with aged rats," *J. Neurosci. Methods*, vol. 121, no. 2, pp. 129–137, 2002.

[9] C. Chang and G. Glover, "Time-frequency dynamics of resting-state brain connectivity measured with fMRI," *NeuroImage*, vol. 50, no. 1, pp. 81–98, 2010.

[10] D. Handwerker *et al.*, "Periodic changes in fMRI connectivity," *NeuroImage*, vol. 63, no. 3, pp. 1712–1719, 2012.

[11] C. Chang *et al.*, "Eeg correlates of time-varying bold functional connectivity," *NeuroImage*, vol. 15, no. 72, pp. 227–236, 2013.

[12] R. Hutchison *et al.*, "Dynamic functional connectivity: Promise, issues, and interpretations," *NeuroImage*, vol. 80, pp. 360–378, 2013.

[13] G. Thompson *et al.*, "Short time windows of correlation between large scale functional brain networks predict vigilance intra-individually and inter-individually," *Hum. Brain Mapping*, vol. 34, no. 12, pp. 3280–3298, 2013.

[14] R. Wilson *et al.*, "Influence of epoch length on measurement of dynamic functional connectivity in wakefulness and behavioural validation in sleep," *NeuroImage*, vol. 112, pp. 169–179, 2015.

[15] A. Allen *et al.*, "Tracking whole-brain connectivity dynamics in the resting state," *Cerebral Cortex*, vol. 24, no. 3, pp. 663–676, 2014.

[16] S. Smith *et al.*, "Temporally-independent functional modes of spontaneous brain activity," *Proc. Nat. Acad. Sci.*, vol. 109, no. 8, pp. 3131–3136, 2012.

[17] U. Sakoglu *et al.*, "A method for evaluating dynamic functional network connectivity and task-modulation: Application to schizophrenia," *MAGMA*, vol. 23, pp. 351–366, 2010.

[18] R. Smith *et al.*, "Wavelet-based regularity analysis reveals recurrent spatiotemporal behavior in resting-state fMRI," *Hum. Brain Mapping*, vol. 36, no. 9, pp. 3603–3620, 2015.

[19] M. Yaesoubi *et al.*, "Dynamic coherence analysis of resting fMRI data to jointly capture state-based phase, frequency, and time-domain information," *NeuroImage*, vol. 120, pp. 133–142, 2015.

[20] J. Shine *et al.*, "Estimation of dynamic functional connectivity using multiplicative analytical coupling," *NeuroImage*, vol. 122, pp. 399–407, 2015.

[21] M. Lindquist *et al.*, "Evaluating dynamic bivariate correlations in resting-state fMRI: A comparison study and a new approach," *NeuroImage*, vol. 101, pp. 531–546, 2014.

[22] B. Rashid *et al.*, "Classification of schizophrenia and bipolar patients using static and dynamic resting-state fMRI brain connectivity," *NeuroImage*, vol. 134, pp. 645–657, 2016.

[23] C. Chang *et al.*, "Tracking brain arousal fluctuations with fMRI," *Proc. Nat. Acad. Sci.*, vol. 113, no. 16, pp. 4518–4523, 2016.

[24] E. Hansen *et al.*, "Functional connectivity dynamics: Modeling the switching behavior of the resting state," *NeuroImage*, vol. 105, pp. 525–535, 2015.

[25] Z. Shi *et al.*, "Realistic models of apparent dynamic changes in resting-state connectivity in somatosensory cortex," *Hum. Brain Mapping*, vol. 37, pp. 3897–3910, 2016.

[26] V. Raatikainen *et al.*, "Combined spatiotemporal ICA (stICA) for continuous and dynamic lag structure analysis of MREG data," *NeuroImage*, vol. 148, pp. 352–68, 2017.

[27] L. Deng *et al.*, "Characterizing dynamic local functional connectivity in the human brain," *Sci. Rep.*, 2016.

[28] M. Dixon *et al.*, "Interactions between the default network and dorsal attention network vary across default subsystems, time, and cognitive states," *NeuroImage*, vol. 147, p. 632–649, 2017.

[29] C. Trapp *et al.*, "On the detection of high frequency correlations in resting state fMRI," *NeuroImage*, 2017.

[30] Y. Ma *et al.*, "Dynamic connectivity patterns in conscious and unconscious brain," *Brain Connectivity*, vol. 7, no. 1, pp. 1–12, 2017.

[31] R. Laughlin *et al.*, "Correlative gene expression to protective seroconversion in rift valley fever vaccinates," *PLOS ONE*, vol. 11, no. 1, 2016.

[32] W. Du *et al.*, "Edge detection in potential filed using the correlation coefficients between the average and standard deviation of vertical derivatives," *J. Appl. Geophys.*, vol. 143, pp. 231–238, 2017.

[33] M. Kafashan *et al.*, "Sevoflurane alters spatiotemporal functional connectivity motifs that link resting-state networks during wakefulness," *Frontiers Neural Circuits*, vol. 147, p. 632–649, 2016.

[34] R. Hindriks *et al.*, "Can sliding-window correlations reveal dynamic functional connectivity in resting-state fMRI?," *NeuroImage*, vol. 127, pp. 242–256, 2016.

[35] M. Weeks, *Digital Signal Processing Using MATLAB & Wavelets*. Boston, MA, USA: Jones & Bartell, 2011.

[36] N. Tzourio-Mazoyer *et al.*, "Automated anatomical labeling of activations in SPM using a macroscopic anatomical parcellation of the MNI MRI single-subject brain," *Magn. Reson. Med.*, vol. 15, no. 1, pp. 273–289, 2002.

[37] W. Shirer *et al.*, "Decoding subject-driven cognitive states with whole-brain connectivity patterns," *Cereb Cortex*, vol. 22, no. 1, pp. 158–165, 2012.

[38] D. Prichard and J. Theiler, "Generating surrogate data for time series with several simultaneously measured variables," *Phys. Rev. Lett.*, vol. 73, no. 7, pp. 951–954, 1994.

[39] E. Norden and Z. Wu, "A review on Hilbert-Huang transform: Method and its applications to geophysical studies," *Rev. Geophys*, vol. 46, no. 2, 2008.

[40] S. Shakil *et al.*, "Adaptive change point detection of dynamic functional connectivity networks," in *Proc. 38th Annu. Int. Conf. IEEE Eng. Med. Biol. Soc.*, 2016, pp. 1135–1138.